Energy Levels and Crystal-Field Calculations of Neodymium in Yttrium Aluminum Garnet*

J. A. KONINGSTEIN AND J. E. GEUSIC

Bell Telephone Laboratories, Murray Hill, New Jersey

(Received 1 June 1964)

Experimental and theoretical studies of the Nd^{3+} spectrum in yttrium aluminum garnet are reported in the present article. From the crystal-field calculations on various J manifolds, it is concluded that the crystal field is approximately tetragonal. The agreement between observed and calculated splitting patterns for J manifolds in which J mixing is small is satisfactory. Our best evaluation of the crystal-field parameters yields: $A_2^0 = 270$ cm^{-1}, $A_4^0 = -250$ cm^{-1}, $A_4^4 = 1250$ cm^{-1}, $A_6^0 = 92$ cm^{-1}, and $A_6^4 = -965$ cm^{-1}.

I. INTRODUCTION

IN the last decade there has been a wide interest in the application of crystal-field theory to the splitting of J manifolds of rare-earth ions in various host lattices. The results have been very encouraging.[1,2] Although the energy levels of some of the rare-earth ions in yttrium aluminum garnet (YAlG) and yttrium gallium garnet (YGaG) are reported in the literature,[3-7] no satisfactory theoretical interpretation has been presented. For example, Pappalardo[6] has attempted to explain the Er^{3+}:YGaG spectrum by considering the crystal field to be of cubic symmetry. The crystallographic data on the positions of ions in yttrium iron garnet (YIG) by Geller and Gilleo,[8] however, indicate that yttrium ions (which can be replaced by rare-earth ions) occupy sites of orthorhombic symmetry. Dillon and Walker,[9] assuming point charges, calculated the crystal-field potential for this site in YIG. Unfortunately, such x-ray data are not available for YAlG or YGaG, but it is reasonable to expect that the site will still be orthorhombic. We have made a detailed study of energy levels of trivalent rare-earth ions in these host lattices. In this communication we discuss the energy-level diagram of Nd^{3+}:YAlG. Our calculations indicate that the symmetry of the crystal field is indeed lower than cubic; however, the experimental results can be described with a crystal field of near tetragonal symmetry.

II. EXPERIMENTAL PROCEDURE

Absorption and fluorescence spectra of Nd^{3+}:YAlG have been studied in the visible, as well as in the infrared at 300°K and at 4.2°K. A Beckman IR7 spectrophotometer with NaCl optics was used to study the absorption spectra in the infrared. A ½-m Jarrell-Ash

[1] G. H. Dieke and H. M. Crosswhite, Appl. Optics 2, 7, 675 (1963).
[2] J. D. Axe and G. H. Dieke, J. Chem. Phys. 37, 2364 (1962).
[3] R. Pappalardo and D. L. Wood, J. Chem. Phys. 33, 1734 (1960).
[4] D. L. Wood, J. Chem. Phys. 39, 1671 (1963).
[5] S. P. Keller and G. D. Petit, Phys. Rev. 121, 1639 (1961).
[6] R. Pappalardo, Z. Physik 173, 374–391 (1963).
[7] R. Pappalardo, Nuovo Cimento 26, 4, 748 (1962).
[8] S. Geller and M. A. Gilleo, Phys. Chem. Solids 3, 30 (1957).
[9] J. F. Dillon and L. R. Walker, Phys. Rev. 124, 1401 (1961).

spectrometer with a resolution of 1 Å was used to record the absorption spectrum in the region 4000 to 12 000 Å. The fluorescence spectrum was studied with a 1-m Jarrell-Ash spectrometer. The samples of Nd^{3+}:$Y_3Al_2(AlO_4)_3$ which were studied contained 5–10 at.% Nd^{3+}.

III. EXPERIMENTAL RESULTS

The positions of the J manifolds of Nd^{3+} are given in a paper by Dieke and Crosswhite.[1] Transitions in the absorption spectrum of Nd^{3+}:YAlG at 4.2°K originate predominantly in the lower level of the $^4I_{9/2}$ manifold. The positions of the excited states are thus directly obtained from the absorption measurements at 4.2°K. The observed infrared and visible absorption spectra are discussed in Secs. III.a and III.b. The position of lines in the spectrum depend on temperature; however, the temperature shifts are relatively small (≤ 10 cm^{-1}). We have used the room-temperature fluorescence data and the helium temperature absorption data to evaluate in a later section crystal-field parameters which are averages over the range 4.2–300°K.

III.a. Absorption Spectrum of Nd^{3+} in the Infrared

Three groups of transitions have been observed in the absorption spectrum at 4.2°K between 2000 and 6800 cm^{-1}. These originate from the lowest level of the $^4I_{9/2}$ state and terminate on crystal-field levels of the $^4I_{11/2}$, $^4I_{13/2}$, and $^4I_{15/2}$ manifolds. The transitions to the $^4I_{11/2}$, $^4I_{13/2}$, and $^4I_{15/2}$ states are found between 2000–2550 cm^{-1}, 3800–4600 cm^{-1}, and 5700–6000 cm^{-1}, respectively. The individual transitions to these manifolds are given in Table I. The results show that the $(J+\frac{1}{2})$-fold degeneracy is completely removed from the $^4I_{11/2}$ state. This indicates that the symmetry of the crystal field is low. The lines in the three groups decrease in intensity as the wave-number position of the transitions increase.

III.b. Absorption Spectrum of Nd^{3+}: YAlG in the Near Infrared and Visible

In the near infrared, two lines of medium intensity are observed at 8757 and 8686 Å. These are due to

TABLE I. The absorption spectrum of Nd^{3+}:YAlG between 2000 and 20 800 cm^{-1} at 4.2°K.

Absorptions at 4.2°K (cm^{-1})	Assignment	Number of Stark components
2010	$^4I_{11/2}$	6
2037		
2111		
2146		
2473		
2526		
3875	$^4I_{13/2}$	6
3985		
4010		
4032		
4490		
4560		
5770	$^4I_{15/2}$	7
5824		
5948		
5978		
6585		
6645		
6755		
11 419	$^4F_{3/2}$	2
11 511		
12 369	$^4F_{5/2}$	3
12 427		
12 517		
12 572	$^2H_{9/2}$	5
12 605		
12 621		
12 820		
12 873		
13 371	$^4F_{7/2}+{}^4S_{3/2}$	6
13 435		
13 563		
13 570		
13 594		
13 633		
14 638	$^4F_{9/2}$	5
14 689		
14 797		
14 826		
14 919		
15 745	$^2H_{11/2}$	6
15 833		
15 867		
15 952		
16 091		
16 105		
16 852	$^2G_{7/2}+{}^4G_{5/2}$	7
16 989		
17 044		
17 241		
17 263		
17 322		
17 570		
18 784	$^2K_{13/2}+{}^4G_{7/2}+{}^2G_{9/2}$	6
18 823		
18 839		
18 985		
19 470		
19 569		
20 718	$^2K_{15/2}$	3
20 761		
20 783		
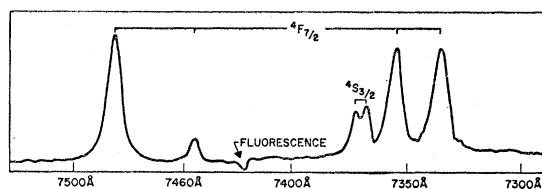
FIG. 1. The absorption spectrum of Nd^{3+}:YAlG between 7300 and 7500 Å at 4.2°K.

transitions between the ground state and the crystal levels of the $^4F_{3/2}$ state. Transition to all possible levels of the $^4F_{5/2}$ and $^2H_{9/2}$ states are found between 8100 and 7700 Å. The transitions to the three levels of the $^4F_{5/2}$ state and to three of the Stark components of $^2H_{9/2}$ show up as strong absorptions.

Six strong absorptions are observed between 7500 and 7300 Å (Fig. 1). According to the energy-level diagram of the Nd^{3+} ion, one expects to find transitions to levels of the $^4F_{7/2}$ and $^4S_{3/2}$ states in that region. If the degeneracy of J manifolds is removed (with the exception of Kramer's degeneracy), one expects for $J=\frac{7}{2}$ and $J=\frac{3}{2}$ states a total of six levels. If the $J=\frac{3}{2}$ state is pure $^4S_{3/2}$, it cannot be split by a crystal field. However, from the calculations of Wybourne,[10] it is known that the "$^4S_{3/2}$" state of Nd^{3+}:YAlG is not a pure S state. The splitting of the $^4S_{3/2}$ state is shown in Fig. 1. Transitions from the ground state to the five levels of the $^4F_{9/2}$ manifold are observed between 6850 and 6650 Å. All five absorptions are observed to the $^2H_{11/2}$ manifold. These occur between 6350 and 6200 Å. The six strong absorptions between 5800 and 5700 Å belong probably to transitions to some of the levels of the $^2G_{7/2}$ and $^4G_{5/2}$ states.

Two groups of bands are recorded in the regions of 5350–5250 Å and 5150–4700 Å. These are attributed to transitions to the Stark components of the $^2K_{13/2}$, $^4G_{7/2}$, $^2G_{9/2}$, and $^2K_{15/2}$ states.

The positions of many of the crystal-field components of the excited states of Nd^{3+}:YAlG obtained from the absorption spectrum at 4.2°K are listed in Table I.

III.c. Fluorescence Spectrum of Nd^{3+}: YAlG

Fluorescence has been detected between 8600 and 13 410 Å. A high-pressure Osram HBO 500-W mercury light source and a Corning 9853 filter were used for the excitation of the fluorescence spectrum. Ten lines are recorded between 8600 and 9500 Å (Fig. 2). These lines are due to fluorescence which originates in levels of the $^4F_{3/2}$ manifold and terminates on levels of the $^4I_{9/2}$ manifold of Nd^{3+}:YAlG. The lines observed in the fluorescence spectrum appear in pairs which are separated on the average by 88 cm^{-1}. This pairing indicates that the $^4F_{3/2}$ state is split by 88 cm^{-1}. The positions of

[10] B. G. Wyborne, J. Chem. Phys. 32, 639 (1960).

FIG. 2. The room-temperature fluorescence spectrum of Nd³⁺: YAlG between 8600 and 9600 Å. Fluorescence originates in levels of the $^4F_{3/2}$ manifold and terminates on levels of the $^4I_{9/2}$ manifold. The average difference of 88 cm⁻¹ represents the splitting of the $^4F_{3/2}$ manifold of Nd³⁺:YAlG.
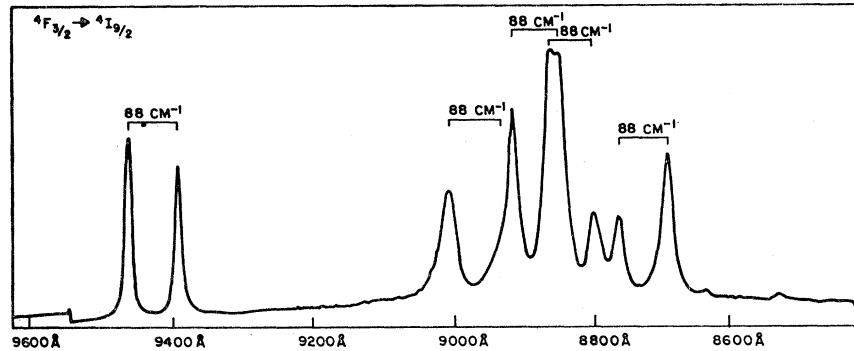
the Stark levels of the $^4I_{9/2}$ state are readily obtained and are given in Table II.

TABLE II. The room-temperature fluorescence spectrum of Nd³⁺:YAlG between 11 502 and 8976 cm⁻¹. Fluorescence originates in the levels of the $^4F_{3/2}$ manifold at 11 502 and 11 414 cm⁻¹ and terminates on levels of the $^4I_{9/2}$ and $^4I_{11/2}$ manifolds of Nd³⁺:YAlG.

Observed fluorescence Series I $\bar{\nu}$ (cm⁻¹)	11 502-$\bar{\nu}$	Observed fluorescence Series II $\bar{\nu}$ (cm⁻¹)	11 414-$\bar{\nu}$	Position of levels of $^4I_{9/2}$ $\bar{\nu}$ (cm⁻¹)
11 502	0	11 414	0	0
11 368	134	11 280	134	134
11 305	197	11 217	197	197
11 191	311	11 103	311	311
10 654	848	10 566	848	848
				$^4I_{11/2}$
9501	2001	9413	2001	2001
9473	2029	9385	2029	2029
9391	2111	9303	2111	2111
9356	2146	9268	2146	2146
9029	2473	8941	2473	2473
8976	2526	8888	2526	2526

Twelve fluorescence lines are observed between 10 750 and 11 080 Å. These are assigned to $^4F_{3/2} \rightarrow {}^4I_{11/2}$ transitions (see Table II). A part of the spectrum is shown in Fig. 3(a), and the energy levels of the $^4I_{11/2}$ state are given in Fig. 3(b). In addition fluorescence has been observed from the $^4F_{3/2}$ levels to the $^4I_{13/2}$ manifold levels; this occurs around 1.3 μ.

IV. THEORETICAL INTERPRETATION OF THE SPECTRUM OF Nd³⁺:YAlG

Our experimental results which are summarized in Tables I and II indicate that most of the J manifolds of Nd³⁺:YAlG are split into the maximum number,[11] $(J+\frac{1}{2})$, of Stark components. We conclude, therefore, that the symmetry of the crystal field, which the Nd³⁺ ion experiences in the YAlG host lattice, is lower than or equal to tetragonal symmetry. Our present theoretical discussion is concerned with an interpretation of the splitting within the J manifolds of Nd³⁺:YAlG due to the crystalline field. This crystalline electric field, which

is produced by the surrounding ions, contributes a term H_c to the total Hamiltonian. H_c can be written as

$$H_c = -e \sum_k V(r_k, \theta_k, \varphi_k) , \qquad (1)$$

where $V(r_k, \theta_k, \varphi_k)$ is the crystal-field potential at the kth $4f$ electron and the summation extends, in this case, over the three $4f$ electrons of Nd³⁺. It is convenient in crystal-field calculations to expand the potential in terms of the spherical harmonics as given below:

$$H_c = \sum_n \sum_{m=-n}^{n} \sum_k B_n{}^m r_k{}^n Y_n{}^m(\theta_k, \varphi_k) . \qquad (2)$$

Here $B_n{}^m$ are constants determined by the positions of the neighboring ions around the central ion, r_k refers to the radius of the kth $4f$ electron, and $Y_n{}^m(\theta_k, \varphi_k)$ are spherical harmonics. For f electrons the only terms which contribute are those with $n \le 6$ and even.

Crystallographic data are not available for the positions of the different ions in YAlG; such data, however, have been reported for YIG.[8,12] The closest neighbors of the yttrium ion (which is replaced by the rare-earth ion) are eight oxygen ions. They are arranged in a distorted cube and give raise to orthorhombic site symmetry at the Y³⁺ ion.

Attempts have been made to calculate the crystal field for YIG. The calculations[9] are based upon a point-charge approximation. The constants $B_2{}^0$, $B_2{}^2$, $B_4{}^0$, $B_4{}^4$, $B_6{}^0$, and $B_6{}^6$, are the important terms, the parameters $B_4{}^2$, $B_6{}^2$, and $B_6{}^6$ are all small. Although the absolute magnitude of these constants are probably different in the aluminum garnet, it is reasonable to assume that their relative magnitudes are approximately the same in both host lattices. Having made this assumption, the perturbing Hamiltonian can then be written as

$$H_c = \alpha [A_2{}^0 Y_2{}^0 + A_2{}^2 (Y_2{}^{+2} + Y_2{}^{-2})]$$
$$+ \beta A_4{}^0 [Y_4{}^0 + 5\delta(Y_4{}^{+4} + Y_4{}^{-4})]$$
$$+ \gamma A_6{}^0 [Y_6{}^0 - 21\epsilon(Y_6{}^{+4} + Y_6{}^{-4})] , \qquad (3)$$

where α, β, and γ are operator equivalent constants de-

[11] H. A. Bethe, Ann. Physik 3, 133 (1929).
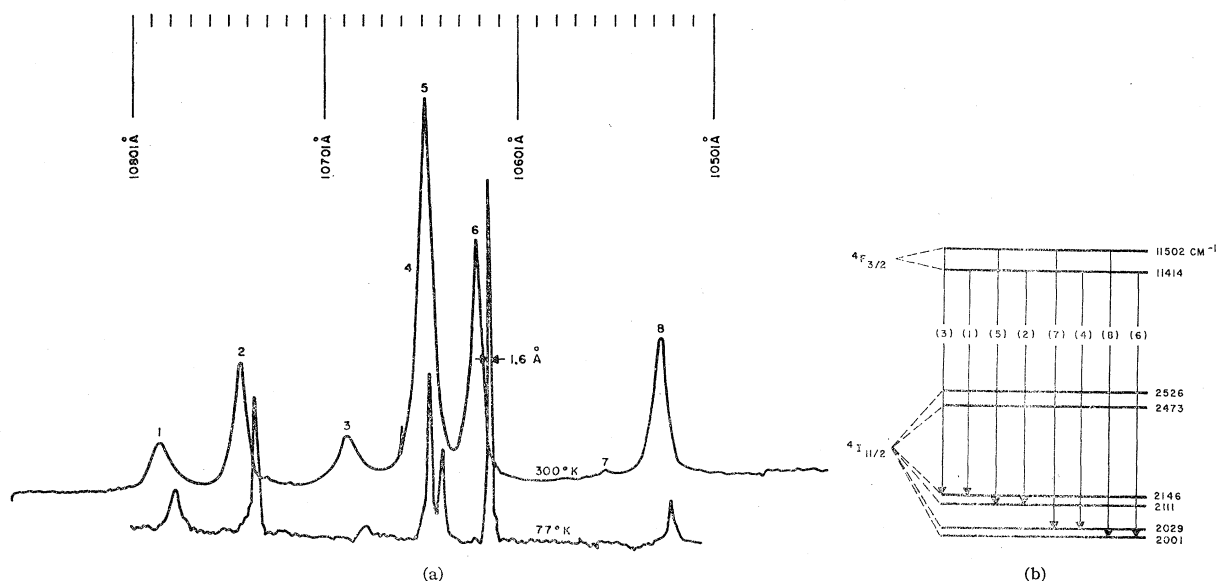
[12] G. Z. Menzer, Kristallografiya 69, 300 (1929).

FIG. 3. (a) The fluorescence spectrum of Nd^{3+} in YAlG at 77 and 300°K in the region of 1.06 μ.
(b) The $^4F_{3/2}$ and $^4I_{11/2}$ energy levels of Nd^{3+} in YAlG for 300°K.

fined by Stevens, Elliott, and Judd,[13–15] and also $A_n{}^m = \langle r^n \rangle B_n{}^m$ with

$$\langle r^n \rangle = \int [R(r)]^2 r^{n+2} dr,$$

$$\delta = A_4{}^4 / 5A_4{}^0, \quad \epsilon = A_6{}^4 / 21A_6{}^0.$$

It may be noted that, for a cubic field,

$$A_2{}^0 = A_2{}^2 = 0, \quad \delta = 1, \quad \epsilon = 1.$$

In calculating the effect of the crystal field described in Eq. (3), we have used the wave functions given by Wybourne[10] for the various J manifolds of Nd^{3+}. His calculations of the wave functions of Nd^{3+} show that some of the J manifolds of Nd^{3+} depart quite drastically from Russell-Saunders coupling. We have used these wave functions to calculate operator equivalent constants for many of the J states of Nd^{3+}; these are given in Table III.

IV.a. Effect of the Second- and Fourth-Order Terms

Crystal-field calculations on the splitting patterns of J manifolds of Eu^{3+} and Tb^{3+}: YAlG indicate[16] that the parameters $A_2{}^0$ are approximately equal for these ions, while also $A_2{}^0 \approx 5A_2{}^2 \approx 265$ cm^{-1}. From the splitting of the $^4F_{3/2}$ manifold of Nd^{3+}: YAlG, a value of $A_2{}^0 = 277$ cm^{-1} can be inferred, while data[17] on the splitting of the

[13] K. W. H. Stevens, Proc. Phys. Soc. (London) A65, 209 (1952).
[14] R. J. Elliott and K. W. H. Stevens, Proc. Roy. Soc. (London) A218, 553 (1953).
[15] B. R. Judd, Proc. Roy. Soc. (London) A227, 552 (1955).
[16] J. A. Koningstein, first following paper, Phys. Rev. 135, A717 (1964).
[17] J. A. Koningstein and J. E. Geusic, second following paper, Phys. Rev. 135, A726 (1926).

$^4S_{3/2}$ state of Er^{3+}: YAlG indicates that $A_2{}^0 \approx 260$ cm^{-1}. In both calculations it is assumed that $A_2{}^0 > A_2{}^2$, which is also found in the cases of Eu^{3+} and Tb^{3+}. We therefore conclude that the value of the parameter $A_2{}^0$ is approximately constant for rare-earth ions in YAlG.

TABLE III. Effective operator equivalent constants for some J states of Nd^{3+}.

Manifold	$\alpha \times 10^3$	$\beta \times 10^3$	$\gamma \times 10^3$
$^4I_{9/2}$	−36.8162	−23.3573	−104.1088
$^4I_{11/2}$	−4.0502	−11.4408	−21.9549
$^4I_{13/2}$	−18.6096	−3.3908	−3.8778
$^4I_{15/2}$	−7.8483	−2.6371	−28.4666
$^4F_{3/2}$	+151.40	...	...
$^4F_{5/2}$	+28.2323	+82.5740	...
$^4F_{7/2}$	+36.5130	+10.8066	−111.3777
$^4F_{9/2}$	+40.1760	−17.7146	−5.7358
$^4S_{3/2}$	+15.200	...	...
$^4G_{5/2}$	+6.5915	+249.2206	...
$^2G_{7/2}$	+11.0249	−1.4783	+43.4223

The positions of the crystal-field components of the $^4F_{5/2}$ manifold of Nd^{3+}: YAlG are determined only by the second- and fourth-order terms. These energy levels are related to the eigenvalues of a 3×3 matrix which can be written as

$$\lambda_{1,2} = \frac{a_{11} + a_{22}}{2} \pm \frac{a_{11} - a_{22}}{2} \left(1 + \frac{4a_{15}^2}{(a_{11} - a_{22})^2} \right)^{1/2}, \quad (4a)$$

$$\lambda_3 = a_{33}, \quad (4b)$$

where

$$a_{11} = 10\alpha A_2{}^0 + 60\beta A_4{}^0, \quad (5a)$$

$$a_{22} = -2\alpha A_2{}^0 - 180\beta A_4{}^0, \quad (5b)$$

$$a_{33} = -8\alpha A_2{}^0 + 120\beta A_4{}^0, \quad (5c)$$

and

$$a_{15} = 5(5)^{1/2}\beta\delta. \quad (5d)$$

Here α and β are the operator equivalent constants. A linear relation between the parameter $A_2{}^0$ and $A_4{}^0$ exists if the eigenvalue interval

$$[(\lambda_1 + \lambda_2)/2] - \lambda_3 = 12\alpha A_2{}^0 - 180\beta A_4{}^0 \quad (6)$$

can be associated with the experimental splitting of the $J = \frac{5}{2}$ manifold. The eight coordinated site of rare-earth ions in garnet systems suggest[18] that the parameter $A_4{}^0$ is less than zero and $A_6{}^0$ is greater than zero. The linear relation given by Eq. (6) between $A_2{}^0$ and $A_4{}^0$, as inferred from the splitting of the $^4F_{5/2}$ manifold of Nd^{3+}:YAlG, is shown in Fig. 4. The plot of $\delta = A_4{}^4/5A_4{}^0$ against the parameter $A_2{}^0$, as calculated from the eigenvalue interval $\lambda_1 - \lambda_2$, is also shown in Fig. 4. It is interesting to note that one evaluates from Fig. 4 that $A_2{}^0 = 270$ cm^{-1} for $\delta = 1$.

The splitting of the $^2F_{5/2}$ manifold of Yb^{3+}:YAlG is given in a paper by Pappalardo and Wood.[3,4] Assuming $\delta = 1$ for the YAlG lattice, we calculate from their data $A_2{}^0 = 278$–312 cm^{-1}. The uncertainty in determining the value of $A_2{}^0$ for Yb^{3+} is due to the fact that absorption spectrum can be interpreted in a number of different ways and because $A_2{}^2$ was not included in the calculation.
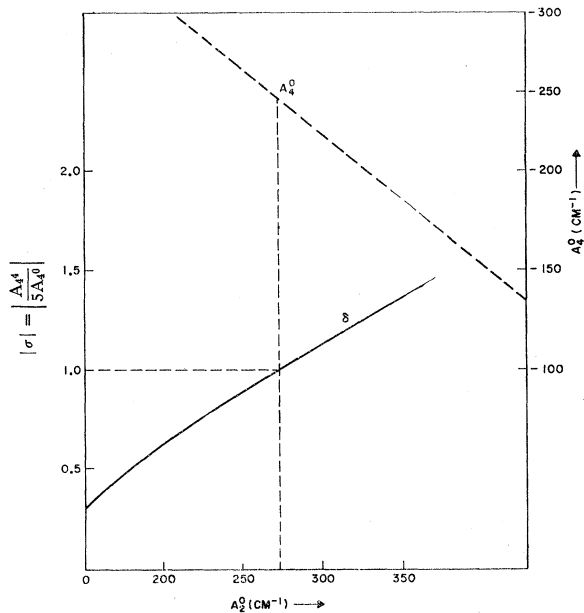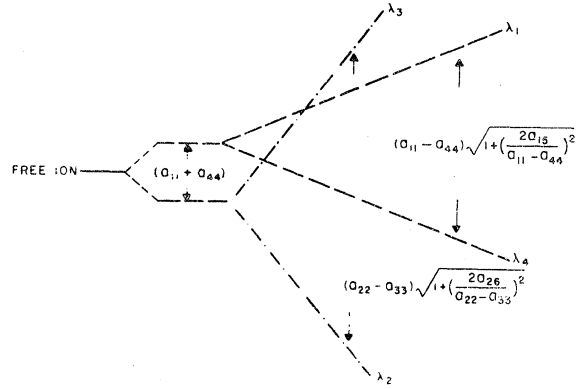

FIG. 5. The splitting of a $J = \frac{7}{2}$ manifold. The meaning of the symbols are given in the text in the beginning of Sec. IV.b.

IV.b. Effect of the Sixth-Order Terms

The sixth-order terms are most easily evaluated from an analysis of the splitting of a $J = \frac{7}{2}$ manifold. The positions of the levels of the $J = \frac{7}{2}$ manifold are related to the crystal-field parameters in the following manner:

$$\lambda_{1,4} = \frac{a_{11} + a_{44}}{2} \pm \frac{a_{11} - a_{44}}{2}\left[1 + \left(\frac{2a_{15}}{a_{11} - a_{44}}\right)^2\right]^{1/2}, \quad (7a)$$

$$\lambda_{2,3} = \frac{a_{22} + a_{33}}{2} \pm \frac{a_{22} - a_{33}}{2}\left[1 + \left(\frac{2a_{26}}{a_{22} - a_{33}}\right)^2\right]^{1/2}, \quad (7b)$$

where

$$a_{11} = 21\alpha A_2{}^0 + 420\beta A_4{}^0 + 1260\gamma A_6{}^0,$$

$$a_{22} = 3\alpha A_2{}^0 - 780\beta A_4{}^0 - 6300\gamma A_6{}^0,$$

$$a_{33} = -9\alpha A_2{}^0 - 180\beta A_4{}^0 + 11\,340\gamma A_6{}^0,$$

$$a_{44} = -15\alpha A_2{}^0 + 540\beta A_4{}^0 - 6300\gamma A_6{}^0,$$

$$a_{15} = 35^{1/2}\beta\delta A_4{}^0 + 3 \cdot 35^{1/2}\gamma\epsilon A_6{}^0,$$

$$a_{26} = 5 \cdot 3^{1/2}\beta\delta A_4{}^0 - 7 \cdot 3^{1/2}\gamma\epsilon A_6{}^0.$$

The following relation is valid:

$$a_{11} + a_{44} = -(a_{22} + a_{33}). \quad (7c)$$

The splitting of a $J = \frac{7}{2}$ manifold as described by (7a), (7b), and (7c) is schematically given in Fig. 5. Using the above expressions and the experimental splitting of the $^4F_{7/2}$ manifold of Nd^{3+}:YAlG, we have calculated the parameter $A_6{}^0$ and the constant $\epsilon = A_6{}^4/21A_6{}^0$ [see Eq. (3)]. In employing values of the parameters $A_2{}^0$, $A_4{}^0$, and $\delta = A_4{}^4/5A_4{}^0$, as obtained from the splitting of the other manifolds, we obtain $A_6{}^0 = 82$–94 cm^{-1} and $\epsilon = 0.50$–0.53. The value of $A_6{}^0 = 92$ cm^{-1} and $\epsilon = 0.50$ gives the best agreement with the splitting of the $^4F_{9/2}$ manifold of Nd^{3+}:YAlG. Our best estimate for the crystal-field parameters of Nd^{3+}:YAlG are given in Table IV, the calculated and observed splittings of the $^4S_{3/2}$, $^4F_{3/2}$, $^4F_{5/2}$, $^4F_{7/2}$, and $^4F_{9/2}$ manifolds are compared, in Fig. 6. Such a comparison of the $^4I_{9/2}$, $^4I_{11/2}$, $^4I_{13/2}$, and

FIG. 4. The dependence of $A_4{}^0$ and $|\delta| = |A_4{}^4/5A_4{}^0|$ as a function of $A_2{}^0$ as obtained from the splitting of the $^4F_{5/2}$ manifold of Nd^{3+}:YAlG.

[18] K. R. Lea, M. J. M. Leask, and W. P. Wolf, Phys. Chem. Solids 23, 1381 (1962).

TABLE IV. Crystal-field parameters for $Nd^{3+}:Y_3Al_2(AlO_4)_3$.

$A_2{}^0=270$ cm^{-1}	$A_4{}^0=-250$ cm^{-1}	$A_6{}^0=92$ cm^{-1}
	$A_4{}^4=1250$ cm^{-1}	$A_6{}^4=-965$ cm^{-1}

$^4I_{15/2}$ manifolds is shown in Fig. 7. The fit for the ^4F manifolds appears to be quite satisfactory. For the ^4I manifolds, the calculated over-all splitting is smaller than observed. The fit is better for the $^4I_{9/2}$ and $^4I_{15/2}$ manifolds than it is for the $^4I_{11/2}$ and $^4I_{13/2}$ manifolds. This is probably due to a greater degree of J mixing in the $^4I_{11/2}$ and $^4I_{13/2}$ manifolds.

V. CONCLUSION

Our results indicate that for $Nd^{3+}:YAlG$ the crystal field has approximately tetragonal symmetry. It is

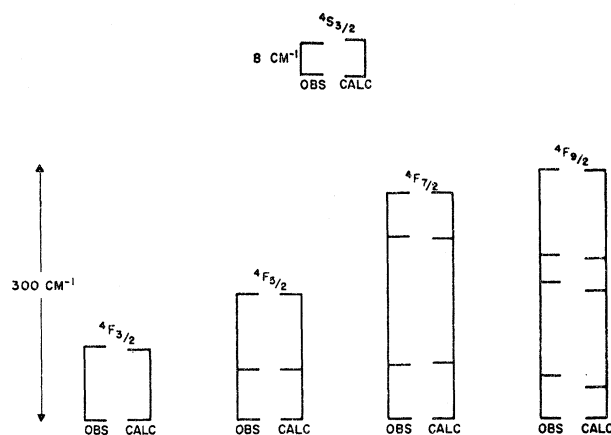FIG. 7. Calculated and observed splittings of the ^4I manifolds of $Nd^{3+}:YAlG$.

FIG. 6. Calculated and observed splitting patterns of the $^4S_{3/2}$, $^4F_{3/2}$, $^4F_{5/2}$, $^4F_{7/2}$, and $^4F_{9/2}$ manifolds of $Nd^{3+}:YAlG$.

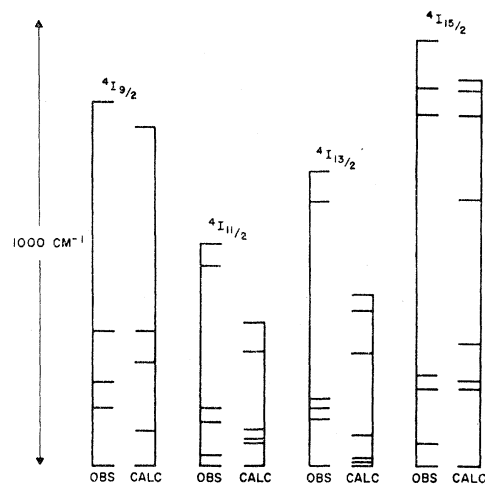perhaps worthwhile noting that even though the splitting of the J manifolds of $Nd^{3+}:YAlG$ is quite large, a reasonable fit of the observed splitting patterns is obtained for manifolds in which J mixing is small.